Precise predictions for $B \to X_c \tau \bar{\nu}$ decay distributions

Zoltan Ligeti[1] and Frank J. Tackmann[2]

[1] *Ernest Orlando Lawrence Berkeley National Laboratory, University of California, Berkeley, CA 94720*
[2] *Theory Group, Deutsches Elektronen-Synchrotron (DESY), D-22607 Hamburg, Germany*

We derive precise standard model predictions for the dilepton invariant mass and the τ energy distributions in inclusive $B \to X_c \tau \bar{\nu}$ decay. We include $\Lambda_{\rm QCD}^2 / m_b^2$ and α_s corrections using the $1S$ short-distance mass scheme, and estimate shape function effects near maximal τ energy. These results can improve the sensitivity of $b \to c \tau \bar{\nu}$ related observables to beyond standard model physics.

I. INTRODUCTION

Recently, B decays mediated by $b \to c \tau \bar{\nu}$ transitions have received renewed attention due to improved measurements of the $\bar{B} \to D \tau \bar{\nu}$ and $\bar{B} \to D^* \tau \bar{\nu}$ decay rates [1], consistent with earlier published [2, 3] and preliminary [4] results. Considering the ratios ($\ell = e, \mu$)

$$R(X) = \frac{\mathcal{B}(B \to X \tau \bar{\nu})}{\mathcal{B}(B \to X \ell \bar{\nu})}, \qquad (1)$$

the combination of the BaBar results

$$R(D^*) = 0.332 \pm 0.030, \qquad R(D) = 0.440 \pm 0.072, \quad (2)$$

gives a more than 3σ deviation [1] from the standard model (SM), which could indicate new physics that couples non-universally to leptons, due to $m_\tau \gg m_{e,\mu}$. The isospin-constrained fit for the branching ratios yields [1]

$$\mathcal{B}(\bar{B} \to D^* \tau \bar{\nu}) + \mathcal{B}(\bar{B} \to D \tau \bar{\nu}) = (2.78 \pm 0.25)\, \% \, . \quad (3)$$

(This average applies for B^- decay [1]; recall the lifetime difference of $B^\pm$ and B^0.)

A recent update of the SM prediction for $R(X_c)$, the ratio for inclusive decay rates, yields [5]

$$R(X_c) = 0.223 \pm 0.005, \qquad (4)$$

which, combined with the world average, $\mathcal{B}(B^- \to X_c e \bar{\nu}) = (10.92 \pm 0.16)\%$ [6, 7], yields [5]

$$\mathcal{B}(B^- \to X_c \tau \bar{\nu}) = (2.42 \pm 0.06)\% \, . \qquad (5)$$

This prediction is rather precise, thus the inclusive measurement can provide information complementary to those from the exclusive modes.

The results in Eq. (3) are in some tension with the LEP average of the rate of an admixture of b-flavored hadrons to decay to τ leptons [8]

$$\mathcal{B}(b \to X \tau^+ \nu) = (2.41 \pm 0.23)\% \, . \qquad (6)$$

This rate has not been measured since the LEP experiments. Neither are theoretical predictions available for $B \to X \tau \bar{\nu}$ decay distributions using a well-defined short-distance quark mass scheme. Such predictions are necessary to provide the best theoretical inputs for future experimental measurements. Measuring the inclusive rate

should be possible using the existing B factory data, and especially using the future Belle II data set [9].

In the future, the uncertainties of the individual $\bar{B} \to D^{(*)} \tau \bar{\nu}$ branching ratios are expected to be reduced to about 2% by Belle II [10], while the uncertainties of the ratios in Eq. (2) may become even smaller. Clearly, both inclusive and exclusive measurements should be pursued.

II. THE OPE RESULTS

Inclusive semileptonic B decay rates can be computed model independently in an operator product expansion (OPE) in terms of local heavy-quark operators (for a review, see Ref. [11]). The leading order reproduces the free-quark decay result, and perturbative and nonperturbative corrections can be systematically incorporated.

The triple differential distribution has been derived, including the leading nonperturbative corrections of order $\Lambda_{\rm QCD}^2 / m_b^2$, in Refs. [12–14]. We use the dimensionless kinematic variables

$$\hat{q}^2 = \frac{q^2}{m_b^2}, \qquad v \cdot \hat{q} = \frac{v \cdot q}{m_b}, \qquad y = \frac{2E_\tau}{m_b}, \qquad (7)$$

where $q = p_\tau + p_\nu$ is the dilepton momentum, v is the four-momentum of the B meson $[(1, \vec{0})$ in the B rest frame], and $E_\tau = v \cdot p_\tau$ is the τ energy measured in the B-meson rest frame. The mass parameters are defined as

$$\rho_\tau = \frac{m_\tau^2}{m_b^2}, \qquad x_\tau = \frac{m_\tau^2}{q^2} = \frac{\rho_\tau}{\hat{q}^2}, \qquad \rho = \frac{m_c^2}{m_b^2}. \qquad (8)$$

It is convenient to define

$$y_\pm = \frac{1}{2}\Big(y \pm \sqrt{y^2 - 4\rho_\tau}\,\Big). \qquad (9)$$

Then $y_+ y_- = \rho_\tau$, and $\{y_+, y_-\} \to \{y, 0\}$ as $m_\tau \to 0$.

The triple differential decay rate in the B rest frame is

$$\frac{1}{\Gamma_0} \frac{d\Gamma}{d\hat{q}^2 \, dy \, dv \cdot \hat{q}}$$
$$= 24\, \theta\big[(2v \cdot \hat{q} - y_+)y_+ - \hat{q}^2\big]\, \theta\big[\hat{q}^2 - (2v \cdot \hat{q} - y_-)y_-\big]$$
$$\times \Big\{ 2(\hat{q}^2 - \rho_\tau)\hat{W}_1 + \big[y(2v \cdot \hat{q} - y) - \hat{q}^2 + \rho_\tau\big]\hat{W}_2$$
$$+ 2\big[\hat{q}^2(y - v \cdot \hat{q}) - \rho_\tau v \cdot \hat{q}\big]\hat{W}_3$$
$$+ \rho_\tau(\hat{q}^2 - \rho_\tau)\,\hat{W}_4 + 2\rho_\tau(2v \cdot \hat{q} - y)\,\hat{W}_5 \Big\}, \quad (10)$$

where

$$\Gamma_0 = \frac{|V_{cb}|^2 \, G_F^2 \, m_b^5}{192\pi^3} \tag{11}$$

is the tree-level free-quark decay rate. The $\hat{W}_i$ are the structure functions of the hadronic tensor [12, 15], which in the local OPE to $\Lambda_{\rm QCD}^2/m_b^2$ contain δ, δ', and δ'' functions of $(1 + \hat{q}^2 - 2v \cdot \hat{q} - \rho)$.

In the literature, only the E_τ spectrum and the total decay rate have been computed including $\Lambda_{\rm QCD}^2/m_b^2$ corrections [12–14] (as well as the τ polarization [12]). These corrections reduce the $B \to X_c \tau \bar{\nu}$ rate by about 7–8%, where about 90% of this reduction is due to the terms proportional to λ_2.

In this paper, we also derive the order $\Lambda_{\rm QCD}^2/m_b^2$ corrections for the q^2 spectrum, as it is expected to be useful for the experimental analysis [9]. While the perturbative corrections were known in the literature in the pole mass scheme, only the total rate was calculated in a short-distance mass scheme in the past. We present results for the first time for the q^2 and E_τ spectra in a well-defined short-distance mass scheme. In addition, we pay special attention to the uncertainties in the end point regions of these spectra, where the local OPE breaks down.

A. Phase space limits

A complication in the massive lepton case is the appearance of the second θ function in Eq. (10), which sets a nontrivial lower limit on $\hat{q}^2$ (which in the $m_\tau \to 0$ limit reduces to $\hat{q}^2 > 0$). Solving the θ functions for the limits on y for fixed $\hat{q}^2$ and $v \cdot \hat{q}$, we have

$$\hat{q}_- + x_\tau \, \hat{q}_+ \le y \le \hat{q}_+ + x_\tau \, \hat{q}_-\,, \tag{12}$$

where

$$\hat{q}_\pm = v \cdot \hat{q} \pm \sqrt{(v \cdot \hat{q})^2 - \hat{q}^2}\,. \tag{13}$$

Substituting the parton level result for $v \cdot \hat{q} = (1 + \hat{q}^2 - \rho)/2$ then gives partonic phase space in the $\hat{q}^2 - y$ plane at tree level. The limits on $\hat{q}^2$ for fixed y are

$$y_- \left(1 - \frac{\rho}{1 - y_-}\right) \le \hat{q}^2 \le y_+ \left(1 - \frac{\rho}{1 - y_+}\right). \tag{14}$$

This is shown in Fig. 1, where we used $\rho = (1.3/4.7)^2$ and $\rho_\tau = (1.777/4.7)^2$ for illustration. The solid (orange) boundary comes from the first θ function in Eq. (10), and the dashed (blue) boundary comes from the second one.

Note that the limits for y are determined by the different θ functions for values of q^2 above and below

$$\hat{q}_0^2 = \sqrt{\rho_\tau} \left(1 - \frac{\rho}{1 - \sqrt{\rho_\tau}}\right). \tag{15}$$

A similar situation occurs in the calculation of the $\mathcal{O}(\alpha_s)$ correction to $d\Gamma/dy \, d\hat{q}^2$ [16], but was not encountered in calculating $\mathcal{O}(\Lambda_{\rm QCD}^2/m_b^2)$ corrections before.
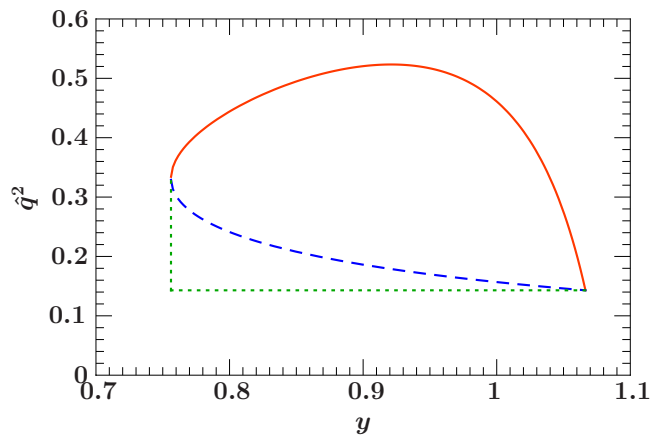

FIG. 1. The $b \to c\tau\bar{\nu}$ Dalitz plot for free quark decay. The solid (orange) boundary comes from the first θ function in Eq. (10), the dashed (blue) boundary from the second one.

Beyond tree level, the lower limit of the $d\hat{q}^2$ integration and the lower limit of dy integration for $\hat{q}^2 < \hat{q}_0^2$ (blue dashed curve in Fig. 1) gets replaced by $\hat{q}^2 > \rho_\tau$ and $y > 2\sqrt{\rho_\tau}$, which is shown by the dotted (green) lines.

Integrating over $\hat{q}^2$, the limits of the y spectrum are

$$2\sqrt{\rho_\tau} < y < 1 + \rho_\tau - \rho\,. \tag{16}$$

Integrating over y, the overall limits of the $\hat{q}^2$ spectrum are

$$\rho_\tau < \hat{q}^2 < (1 - \sqrt{\rho})^2\,. \tag{17}$$

The above are the partonic phase space limits relevant to the OPE result. For the hadronic phase space limits, m_b is replaced by m_B and ρ is replaced by m_D^2/m_B^2.

B. The q^2 spectrum

Since the hadronic structure functions $\hat{W}_i$ are functions of $\hat{q}^2$ and $\hat{v} \cdot q$ only, it is easiest to first integrate the triple differential spectrum in Eq. (10) over the lepton energy with the limits given in Eq. (12). Doing so, we obtain for the double differential spectrum

$$\frac{1}{\Gamma_0} \frac{d\Gamma}{d\hat{q}^2 \, dv \cdot \hat{q}} = 96 \, (1 - x_\tau)^2 \sqrt{(v \cdot \hat{q})^2 - \hat{q}^2} \tag{18}$$

$$\times \left\{ \hat{q}^2 \, \hat{W}_1 + \frac{1}{3}\left[(v \cdot \hat{q})^2 - \hat{q}^2\right](1 + 2x_\tau)\,\hat{W}_2 \right.$$

$$\left. + \frac{\rho_\tau}{2}\left(\hat{W}_2 + \hat{q}^2\hat{W}_4 + 2v \cdot \hat{q}\hat{W}_5\right)\right\}.$$

Substituting the OPE results for the $\hat{W}_i$, we obtain for the q^2 spectrum

$$\frac{1}{\Gamma_0}\frac{d\Gamma}{d\hat{q}^2} = 2(1-x_\tau)^2\sqrt{P^2-4\rho}\left\{\left(1+\frac{\lambda_1+15\lambda_2}{2m_b^2}\right)\right.$$
$$\times\left[3\hat{q}^2 P(1+x_\tau)+(P^2-4\rho)(1+2x_\tau)\right] \quad (19)$$
$$+\frac{6\lambda_2}{m_b^2}\left[(P-2)(1+2x_\tau)+\hat{q}^2(4+5x_\tau)\right.$$
$$\left.\left.+\hat{q}^2\frac{2(2\hat{q}^2+P-2)(2+x_\tau)+3\hat{q}^2 P(1+x_\tau)}{P^2-4\rho}\right]\right\},$$

where we defined $P = 1-\hat{q}^2+\rho$, and we have suppressed the θ functions expressing the $\hat{q}^2$ limits given in Eq. (17). Integrating over $\hat{q}^2$ we reproduce the total rate given in Ref. [12].

As we will see in Sec. III below, the order $\Lambda_{\rm QCD}^2/m_b^2$ corrections reduce the $B\to X_c\tau\bar{\nu}$ rate mainly at higher values of $\hat{q}^2$, dominated by the terms proportional to λ_2. Near maximal $\hat{q}^2$, the λ_2 terms behave as $(\hat{q}_{\rm max}^2-\hat{q}^2)^{-1/2}$, and the differential rate becomes negative. This indicates a breakdown of the OPE; in this region of phase space, the hadronic final state is constrained to be in the resonance region, and the OPE cannot describe the spectrum point by point. Thus, integration over some region of $\Delta\hat{q}^2$ is necessary near maximal $\hat{q}^2$ to obtain a reliable result. The form of Eq. (19) makes it clear that this effect is not related to the b quark distribution function in the B meson, the so-called shape function (which is neither relevant for the high q^2 region in $B\to X_u\ell\bar{\nu}$ [17]). Note also that the difference of the upper limit of q^2 at lowest order in the OPE and at the hadronic level is suppressed by $\Lambda_{\rm QCD}^2$.

C. The τ energy spectrum

To obtain the E_τ spectrum, we substitute the OPE results for the $\hat{W}_i$ in the triple differential rate in Eq. (10). The integration over $v\cdot\hat{q}$ is performed using the $\delta^{(n)}(1+\hat{q}^2-2v\cdot\hat{q}-\rho)$ contained in the $\hat{W}_i$. Next, we integrate over $\hat{q}^2$ with the integration limits in Eq. (14). At leading order we obtain

$$\frac{1}{\Gamma_0}\frac{d\Gamma}{dy} = 2\sqrt{y^2-4\rho_\tau}\,\theta(y-2\rho_\tau)\,\theta(1-R)\,(1-R)^2 \quad (20)$$
$$\times\left[y\rho\frac{1-R}{R}+(1+2R)(y-2\rho_\tau)(2-y)\right],$$

where

$$R = \frac{\rho}{(1-y_+)(1-y_-)} = \frac{\rho}{1-y+\rho_\tau}, \quad (21)$$

and for the $\Lambda_{\rm QCD}^2/m_b^2$ corrections we reproduce the results in Refs. [12–14]. The two θ functions in Eq. (20) correspond to the limits on y in Eq. (16).

As for large values of $\hat{q}^2$, the OPE also breaks down for large values of y. Contrary to the end point of the q^2

spectrum, the E_τ end point does differ by an amount of order $\Lambda_{\rm QCD}$ between the partonic and hadronic phase space limits. If one treats $m_c\sim\mathcal{O}(\sqrt{m_b\Lambda_{\rm QCD}})$, or equivalently $\rho\sim\Lambda_{\rm QCD}/m_b$, then the problematic terms in the OPE that are enhanced near the end point can be resummed, replacing the usual OPE by an expansion in terms of nonlocal light-cone operators, whose matrix elements yield nonperturbative B-meson distribution functions (shape functions). [Such effects would formally be subleading if one treats $m_c^2/m_b^2\sim\mathcal{O}(1)$.] At the lowest order description of the end point region, $\mathcal{O}[(\Lambda_{\rm QCD}/m_b)^0]$, a single shape function appears. This is well known for $B\to X\ell\nu$ decays [18–21]. When carried out appropriately, the shape function OPE can be rendered valid away from the end point region as well, such that it smoothly recovers the local OPE result [22, 23]. For $b\to c$ transitions, this is possible if the OPE is directly performed for the lepton energy spectrum [22]. Following Ref. [22] and including the τ mass, we obtain at leading order

$$\frac{1}{\Gamma_0}\frac{d\Gamma}{dy} = 2\sqrt{y^2-4\rho_\tau}\int d\hat{\omega}\,m_b\,F(m_b\hat{\omega}+m_B-m_b)$$
$$\times\theta(y-2\rho_\tau)\theta(1-R_\omega)\,(1-R_\omega)^2\left\{y\rho\frac{1-R_\omega}{R_\omega}\right.$$
$$\left.+(1+2R_\omega)\left[y-\hat{\omega}y_- -2\rho_\tau\right](2-y-\hat{\omega})\right\}. \quad (22)$$

where

$$R_\omega = \frac{\rho}{(1-y_+-\hat{\omega})(1-y_-)}, \quad (23)$$

and the leading shape function, $F(k)$, in Eq. (22) is defined with the same conventions as in Refs. [23, 24].

For $B\to X_c\tau\nu$, the end point region of the lepton energy spectrum is given by $1-y_+\sim\Lambda_{\rm QCD}/m_b$. The result in Eq. (22) arises from replacing $1-y_+\to 1-y_+-\hat{k}_+$ in the local OPE. (Some overall factors that arise from the leptonic phase space are unaffected.) For small y_+, corresponding to small E_τ, one can expand

$$m_b F(m_b\hat{\omega}+m_B-m_b) = \delta(\hat{\omega})+\dots, \quad (24)$$

which recovers the leading-order result in Eq. (20). In principle, all $\Lambda_{\rm QCD}^2/m_b^2$ corrections in the local OPE at small y_+ can be recovered from the shape function expansion, which would require one to carry it out to the same higher order [23].

D. The $1S$ mass scheme and perturbative corrections

It is well known that the pole mass of a heavy quark is not well defined beyond perturbation theory. This manifests itself, for example, in poorly behaved perturbation series. In this paper, we use the $1S$ mass scheme [25–27]. Including both the c quark and τ lepton mass effects, the

corrections to free-quark decay for the total rate were computed to $\mathcal{O}(\alpha_s)$ [28], $\mathcal{O}(\alpha_s^2\beta_0)$ [29], and $\mathcal{O}(\alpha_s^2)$ [30]. The $\mathcal{O}(\alpha_s)$ result [28] was already used in the numerical prediction for the rate 20 years ago [12], and the $\mathcal{O}(\alpha_s^2\beta_0)$ result [29] could be used to show that the perturbation series in the $1S$ scheme, $1 - 0.070\epsilon - 0.016\epsilon_{\mathrm{BLM}}^2$ [26], is much better behaved than that in the pole scheme, $1 - 0.097\epsilon - 0.064\epsilon_{\mathrm{BLM}}^2$. (Here powers of $\epsilon = 1$ indicate the order in the $1S$ expansion, and $\epsilon_{\mathrm{BLM}}^2$ corresponds to the lowest order term proportional to $\beta_0 = 11 - 2n_f/3$, the first coefficient in the QCD β function.) This improvement in the perturbation series is essential to obtain the precise predictions in Eqs. (4) and (5).

The $\mathcal{O}(\alpha_s)$ correction to $\mathrm{d}\Gamma/\mathrm{d}\hat{q}^2$ was calculated analytically in Ref. [31], while the corrections to the lepton energy spectrum can be obtained by integrating $\mathrm{d}^2\Gamma/\mathrm{d}y\,\mathrm{d}\hat{q}^2$ calculated in Ref. [16]. In particular, the fractional corrections at order α_s to both $\mathrm{d}\Gamma/\mathrm{d}\hat{q}^2$ and $\mathrm{d}\Gamma/\mathrm{d}y$ are remarkably independent of $\hat{q}^2$ and y, and so have very little effect on the shape of the spectra except very close to their end points.

III. NUMERICAL RESULTS

Hereafter we revert to dimensionful kinematic variables, E_τ and q^2 (i.e., no longer rescale them by powers of m_b). The phase space limits for the $\hat{q}^2$ and y distributions are given in Eqs. (17) and (16). Restoring the dimensions of the variables,

$$m_\tau < E_\tau < \frac{m_b^2 - m_c^2 + m_\tau^2}{2m_b},$$
$$m_\tau^2 < q^2 < (m_b - m_c)^2. \qquad (25)$$

One can immediately see, writing

$$m_{b,c} = m_{B,D} - \bar{\Lambda} + \mathcal{O}(\Lambda_{\mathrm{QCD}}^2/m_{b,c}^2), \qquad (26)$$

that the difference of the upper limit of q^2 at lowest order in the OPE, $(m_b - m_c)^2$, and at the hadronic level, $(m_B - m_D)^2$, is suppressed by Λ_{QCD}^2. However, the lepton energy end point does receive an $\mathcal{O}(\Lambda_{\mathrm{QCD}})$ correction, although only about $100\,\mathrm{MeV}$ (it is $\sim 300\,\mathrm{MeV}$ for $B \to X_u e\bar{\nu}$). As explained above, treating $m_c^2/(m_b\Lambda_{\mathrm{QCD}}) \sim \mathcal{O}(1)$ or $m_c^2/m_b^2 \sim \mathcal{O}(1)$ affects whether the shape function is formally relevant to describe the E_τ end point region. We use Eq. (22) to determine beyond which value of E_τ the shape function becomes important and the local OPE result cannot be trusted anymore. A more detailed analysis for $B \to X_u\tau\nu$ will be given elsewhere [32].

The numerical inputs we use are summarized in Table I. For the leading order shape function, we use the fit result from Ref. [33], and for consistency we also take the central value for m_b^{1S} from there, which is consistent with the fit results in the $1S$ scheme in Refs. [7, 34], with a conservative error of $\pm 50\,\mathrm{MeV}$.

In the $1S_{\mathrm{EXP}}$ scheme in Ref. [34], one relates $m_b - m_c$ using heavy-quark effective theory (HQET) to a linear

combination of the spin averaged hadron mass difference, $\overline{m}_B - \overline{m}_D$, λ_1, and dimension-6 HQET matrix elements. This removes the leading renormalon from m_c^{pole} as well. Then writing $m_c = m_b^{1S} - \delta m_{bc}$, and treating $\delta m_{bc} = m_b - m_c$ as an independent parameter is practical, as it is well constrained by measured $B \to X_c\ell\bar{\nu}$ spectra, and is the dominant source of formally $\mathcal{O}(\lambda_1/m_c^2)$ corrections [34]. (Note that the $B \to X_c\ell\bar{\nu}$ data imply that the correlation of these terms with other contributions is very significant.) Numerically, we use the average of the fit results in Refs. [7, 34] and use their difference of $20\,\mathrm{MeV}$ as a conservative error. For λ_1 we use $-0.3\,\mathrm{GeV}^2$ as the central value and vary it by 25%, which covers the values obtained in Refs. [7, 34] and also the somewhat lower value implied by the result we use for the leading shape function. The value of $\lambda_2 = 0.12\,\mathrm{GeV}^2$ is known very well from the $m_{B^*} - m_B$ mass splitting. We also vary it by 25%. The variations for λ_1 and λ_2 can be viewed as an uncertainty estimate to account for the higher-order perturbative corrections to their OPE coefficients (as well as the omitted $\Lambda_{\mathrm{QCD}}^3/m_b^3$ corrections).

Figure 2 shows the predictions for $\mathrm{d}\Gamma/\mathrm{d}q^2$ (left) and $\mathrm{d}\Gamma/\mathrm{d}E_\tau$ (right) in the $1S$ mass scheme for the b quark. The dotted (green) curves show the free-quark decay result, the dashed (blue) curves include $\mathcal{O}(\alpha_s)$ corrections, and the solid (orange) curves include both α_s and $\Lambda_{\mathrm{QCD}}^2/m_b^2$ corrections. The $\Lambda_{\mathrm{QCD}}^2/m_b^2$ corrections are negligible at low values of $\hat{q}^2$ and y, while their effects become important for larger values. For $\mathrm{d}\Gamma/\mathrm{d}q^2$, they drive the spectrum negative near the end point, where the OPE breaks down, as already discussed above. The peculiar shape of $\mathrm{d}\Gamma/\mathrm{d}E_\tau$ including the $\mathcal{O}(\Lambda_{\mathrm{QCD}}^2/m_b^2)$ terms is due to the fact that near the end point both the λ_1 and λ_2 terms are large, and the λ_1 term changes sign. For $\mathrm{d}\Gamma/\mathrm{d}E_\tau$ the dot-dashed (dark red) curve combines the $\mathcal{O}(\alpha_s, \Lambda_{\mathrm{QCD}}^2/m_b^2)$ corrections with the tree-level leading shape function result in Eq. (22) (appropriately avoiding any double counting of $\Lambda_{\mathrm{QCD}}^2/m_b^2$ corrections). The theoretical uncertainty of $\mathrm{d}\Gamma/\mathrm{d}E_\tau$ becomes clearly large for $E_\tau \gtrsim 2.3\,\mathrm{GeV}$, where the result including shape function effects starts to differ noticeably from the local OPE result. On the other hand, for $E_\tau \lesssim 2.2\,\mathrm{GeV}$ the local OPE provides a reliable prediction for the spectrum.

Figure 3 shows the various sources of uncertainties in the results in Fig. 2 from varying the parameters as mentioned above and summarized in Table I. The variations

Parameter	Central value	Variation	$\Delta\Gamma_{\mathrm{total}}$
m_b^{1S}	$4.71\,\mathrm{GeV}$	$\pm 50\,\mathrm{MeV}$	$\pm 5.3\%$
δm_{bc}	$3.40\,\mathrm{GeV}$	$\pm 20\,\mathrm{MeV}$	$\pm 4.4\%$
λ_1	$-0.30\,\mathrm{GeV}^2$	$\pm 25\%$	$\pm 0.2\%$
λ_2	$0.12\,\mathrm{GeV}^2$	$\pm 25\%$	$\pm 2.0\%$
α_s	0.218	$^{+0.065}_{-0.040}$	$\pm 1.1\%$

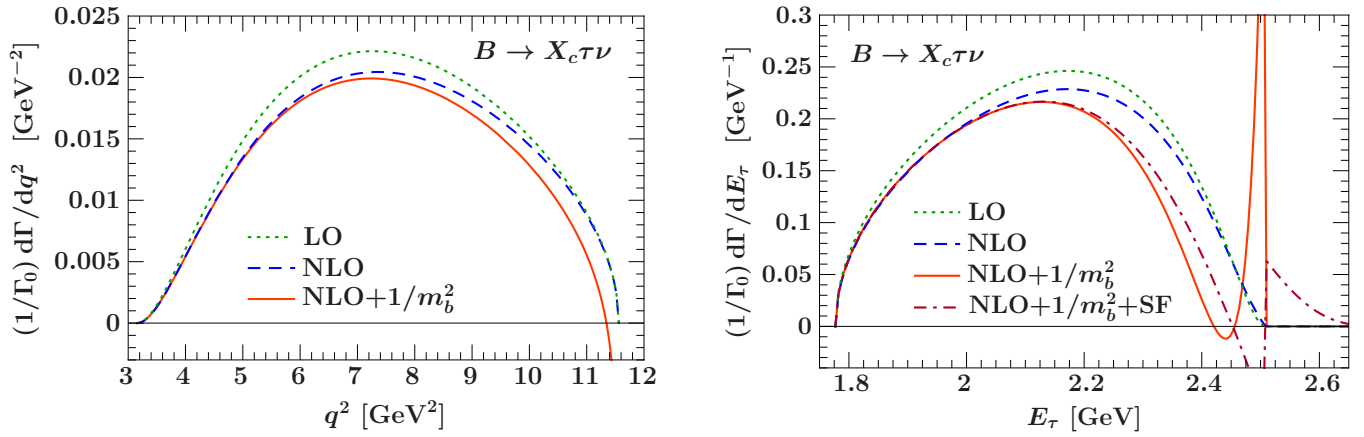TABLE I. Central values of input parameters, their variations, and the resulting uncertainties in the total rate prediction.

FIG. 2. The OPE predictions for the $d\Gamma/dq^2$ (left) and $d\Gamma/dE_\tau$ (right) in $B \to X_c\tau\bar\nu$. The dotted (green) curves show the free-quark decay result, the dashed (blue) curves include $\mathcal{O}(\alpha_s)$ corrections, and the solid (orange) curves include both α_s and $\Lambda_{\rm QCD}^2/m_b^2$ corrections. For $d\Gamma/dE_\tau$ the dot-dashed (dark red) curve combines $\mathcal{O}(\alpha_s, \Lambda_{\rm QCD}^2/m_b^2)$ with the leading-order shape function result.
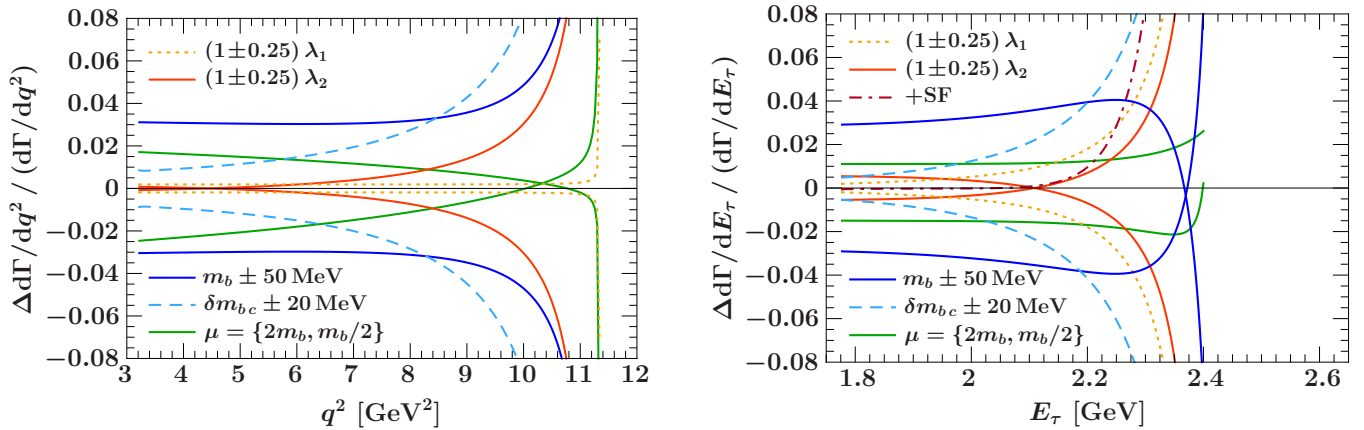

FIG. 3. The fractional uncertainties in the OPE predictions for $d\Gamma/dq^2$ (left) and $d\Gamma/dE_\tau$ (right). The solid blue curves show the effect of the variation of m_b^{1S} by $\pm50\,{\rm MeV}$ (keeping δm_{bc} fixed), the dashed light blue curves show the variation of δm_{bc} by $\pm20\,{\rm MeV}$, the solid green curves show the μ variation between $m_b/2$ and $2m_b$, and the solid red (dotted light orange) curves show the variation of the coefficient of λ_2 (λ_1) by $\pm25\%$. The dot-dashed (dark red) curve shows the relative correction from including the leading shape function.

from m_b keeping δm_{bc} fixed (solid blue curves) and δm_{bc} (dashed light blue curves) dominate at low and high values, respectively. Varying the renormalization scale, μ, between $m_b/2$ and $2m_b$ is shown by the solid green curves, and varying the coefficients of λ_2 and λ_1 are shown by the solid red and dotted light orange curves, respectively. The resulting uncertainties in the total rate from each of these parameter variations are given in Table I. For $d\Gamma/dE_\tau$ we also show the relative corrections due to shape function effects (dark red dot-dashed curve).

Since the largest parts of the uncertainties cancel in the ratio in Eq. (4), yielding a precise SM prediction of the total $B \to X_c\tau\bar\nu$ rate in Eq. (5), and the spectra cannot be calculated reliably point by point near the end points of either $d\Gamma/dq^2$ or $d\Gamma/dE_\tau$, in Fig. 4 we show the

integrated rates above a cut normalized to the total rate,

$$\widehat{\Gamma}(q_{\rm cut}^2) = \frac{1}{\Gamma} \int_{q_{\rm cut}^2} \frac{d\Gamma}{dq^2}\,, \qquad \widetilde{\Gamma}(E_{\rm cut}) = \frac{1}{\Gamma} \int_{E_{\rm cut}} \frac{d\Gamma}{dE_\tau}\,, \quad (27)$$

at different orders in the OPE. The $\mathcal{O}(\alpha_s)$ corrections have a negligible effect on these distributions since they do not affect the shape of the spectra. The yellow band shows the total uncertainty obtained by adding all uncertainties in quadrature. To obtain the individual uncertainties we apply the same variations in both numerator and denominator and take the larger of the up/down variations as the uncertainty. In these normalized event fractions, the m_b and μ variations mostly cancel. The total uncertainty essentially comes from δm_{bc} and λ_2 for $\widehat{\Gamma}(q^2)$, and from δm_{bc} and $\lambda_{1,2}$ for $\widetilde{\Gamma}(E_\tau)$. For $\widehat{\Gamma}(q_{\rm cut}^2)$ the relative uncertainties in the OPE result become very
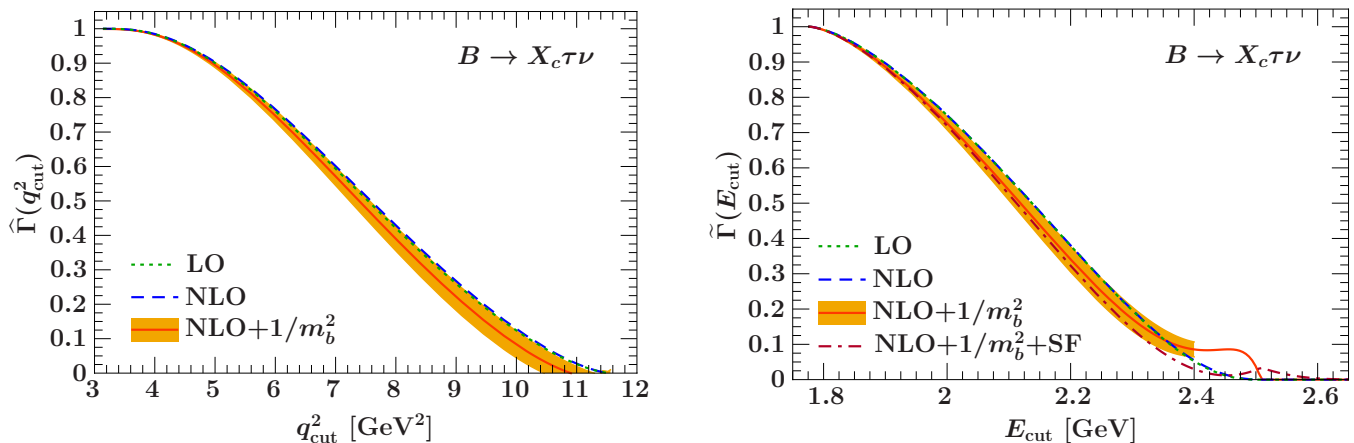
FIG. 4. The OPE predictions for the fraction of events above a certain cut in $d\Gamma/dq^2$ (left) and $d\Gamma/dE_\tau$ (right) in $B \to X_c\tau\bar\nu$. The meaning of the curves is the same as in Fig. 2. The shaded band shows the total uncertainties in the full result.

large beyond $q^2_{\rm cut} \gtrsim 10\,{\rm GeV}^2$, which is as expected. For $\widetilde{\Gamma}(E_{\rm cut})$ the dot-dashed (dark red) curve shows the effect of including the leading shape function. One can also see here that the local OPE result starts to become unreliable beyond $E_{\rm cut} \gtrsim 2.3\,{\rm GeV}$.

IV. SUMMARY AND CONCLUSIONS

We calculated the inclusive $B \to X_c\tau\nu$ decay distributions in τ energy and dilepton invariant mass. Our results for the $\Lambda^2_{\rm QCD}/m_b^2$ corrections to $d\Gamma/dq^2$ are new. We derived predictions for the spectra using the $1S$ short-distance mass scheme, incorporating the $\mathcal{O}(\Lambda^2_{\rm QCD}/m_b^2)$ and $\mathcal{O}(\alpha_s)$ corrections. We also studied the effects of the shape function on the τ energy end point region. The rates can be predicted precisely if one makes no cuts in the regions $q^2 \gtrsim 9\,{\rm GeV}^2$ and $E_\tau \gtrsim 2.2\,{\rm GeV}$.

Recent measurements of the $\bar B \to D\tau\bar\nu$ and $\bar B \to D^*\tau\bar\nu$ decay rates indicate possible deviations from the standard model. The BaBar and Belle measurements of these exclusive modes are consistent with one another, but are in some tension with LEP measurements of the inclusive $B \to X_c\tau\bar\nu$ rate. This makes a new measurement of the inclusive $B \to X_c\tau\bar\nu$ decay rate particularly timely, especially since no results are available from the e^+e^- B factories, and measurements may be possible using the existing data sets. Given the current tensions, measuring $B \to X_c\tau\bar\nu$ will also be important with Belle II data.

Since it might only be possible to measure the inclusive rate in limited regions of phase space, precise theory predictions for differential distributions are required, and the calculations presented here should help to improve the experimental sensitivities.

[1] J. P. Lees *et al.* [BaBar Collaboration], Phys. Rev. Lett. **109**, 101802 (2012) [arXiv:1205.5442].
[2] A. Bozek *et al.* [Belle Collaboration], Phys. Rev. D **82**, 072005 (2010) [arXiv:1005.2302].
[3] B. Aubert *et al.* [BaBar Collaboration], Phys. Rev. Lett. **100**, 021801 (2008) [arXiv:0709.1698].
[4] R. Watanabe, talk at FPCP 2014, Marseille, France, http://indico.cern.ch/event/269618/session/10/contribution/15/material/slides/0.pdf.
[5] M. Freytsis, Z. Ligeti, J. Ruderman, to appear.
[6] F. U. Bernlochner, Z. Ligeti and S. Turczyk, Phys. Rev. D **85**, 094033 (2012) [arXiv:1202.1834].
[7] Y. Amhis *et al.* [Heavy Flavor Averaging Group], arXiv:1207.1158; and updates at http://www.slac.stanford.edu/xorg/hfag/.
[8] J. Beringer *et al.* [Particle Data Group], Phys. Rev. D86, 010001 (2012).
[9] Phillip Urquijo, private communications.
[10] T. Aushev *et al.*, arXiv:1002.5012.
[11] A. V. Manohar and M. B. Wise, Camb. Monogr. Part. Phys. Nucl. Phys. Cosmol. **10**, 1 (2000).
[12] A. F. Falk, Z. Ligeti, M. Neubert and Y. Nir, Phys. Lett. B **326**, 145 (1994) [hep-ph/9401226].
[13] S. Balk, J. G. Korner, D. Pirjol and K. Schilcher, Z. Phys. C **64**, 37 (1994) [hep-ph/9312220].
[14] L. Koyrakh, Phys. Rev. D **49**, 3379 (1994) [hep-ph/9311215].
[15] A. V. Manohar and M. B. Wise, Phys. Rev. D **49**, 1310 (1994) [hep-ph/9308246].

[16] M. Jezabek and L. Motyka, Nucl. Phys. B **501**, 207 (1997) [hep-ph/9701358]; Acta Phys. Polon. B **27**, 3603 (1996) [hep-ph/9609352].

[17] C. W. Bauer, Z. Ligeti and M. E. Luke, Phys. Lett. B **479**, 395 (2000) [hep-ph/0002161]; Phys. Rev. D **64**, 113004 (2001) [hep-ph/0107074].

[18] M. Neubert, Phys. Rev. D **49**, 3392 (1994) [hep-ph/9311325].

[19] A. F. Falk, E. E. Jenkins, A. V. Manohar and M. B. Wise, Phys. Rev. D **49**, 4553 (1994) [hep-ph/9312306].

[20] I. I. Y. Bigi, M. A. Shifman, N. G. Uraltsev and A. I. Vainshtein, Int. J. Mod. Phys. A **09**, 2467 (1994) [hep-ph/9312359].

[21] T. Mannel and M. Neubert, Phys. Rev. D **50**, 2037 (1994) [hep-ph/9402288].

[22] T. Mannel and F. J. Tackmann, Phys. Rev. D **71**, 034017 (2005) [hep-ph/0408273].

[23] F. J. Tackmann, Phys. Rev. D **72**, 034036 (2005) [hep-ph/0503095].

[24] Z. Ligeti, I. W. Stewart and F. J. Tackmann, Phys. Rev. D **78**, 114014 (2008) [arXiv:0807.1926].

[25] A. H. Hoang, Z. Ligeti and A. V. Manohar, Phys. Rev. Lett. **82**, 277 (1999) [hep-ph/9809423].

[26] A. H. Hoang, Z. Ligeti and A. V. Manohar, Phys. Rev. D **59**, 074017 (1999) [hep-ph/9811239];

[27] A. H. Hoang and T. Teubner, Phys. Rev. D **60**, 114027 (1999) [hep-ph/9904468].

[28] Q. Ho-kim and X. Y. Pham, Annals Phys. **155**, 202 (1984).

[29] M. Lu, M. E. Luke, M. J. Savage and B. H. Smith, Phys. Rev. D **55**, 2827 (1997) [hep-ph/9605406].

[30] S. Biswas and K. Melnikov, JHEP **1002**, 089 (2010) [arXiv:0911.4142].

[31] A. Czarnecki, M. Jezabek and J. H. Kuhn, Phys. Lett. B **346**, 335 (1995) [hep-ph/9411282].

[32] Z. Ligeti and F. Tackmann, to appear.

[33] F. U. Bernlochner *et al.* [SIMBA Collaboration], PoS ICHEP **2012**, 370 (2013) [arXiv:1303.0958].

[34] C. W. Bauer, Z. Ligeti, M. Luke, A. V. Manohar and M. Trott, Phys. Rev. D **70**, 094017 (2004) [hep-ph/0408002]; C. W. Bauer, Z. Ligeti, M. Luke and A. V. Manohar, Phys. Rev. D **67**, 054012 (2003) [hep-ph/0210027].